FBR for Catalytic Propylene Polymerization: Controlled Mixing and Reactor Modeling

G. B. Meier, G. Weickert, and W. P. M. van Swaaij
Industrial Polymerization Processes, Process Technology Institute Twente,
University of Twente, 7500 AE Enschede, The Netherlands

Particle mixing and segregation have been studied in a small-scale fluidized-bed reactor (FBR) under pressure. The solids mixing is relatively faster than the residence time of catalyst particles in the case of a polymerization process, but smaller particles accumulate in the upper zone. Semibatch propylene polymerization experiments showed that the vertical temperature gradients are caused mainly by catalyst segregation. At low gas velocities, segregation and mixing can differ under reacting conditions compared to nonreacting conditions due to particle–particle interactions. Catalyst concentration gradients caused by incomplete mixing are strengthened remarkably by the exothermic reaction even at low polymerization rates. These observations do not represent an industrial situation. The FBR has therefore been equipped with a draft tube and cone to control vertical solids mixing. The internal solids circulation rate is a nonlinear function of the gas velocity. Strongly reduced segregation, elutriation, and entrainment observed were compared to experiments without a draft tube. Temperature profiles observed during polymerization can be controlled by the solids circulation rate. Hydrogen injections led to an instantaneously increased polymerization rate, probably due to the reactivation of dormant sites. Irreversible deactivation rates of dormant and active sites seem to be the same. Moreover, hydrogen appeared to be very effective for widening the molecular-weight distribution. A compartment model developed describes the temperature profile in the reactor and related molecular-weight distribution of the polymer.

Introduction

The most widely established industrial gas-phase technology for polyolefin production is the fluidized-bed reactor operating at elevated pressures between 20 and 30 bar. In these large-scale units, bubbles rising from the distributor plate tend to accumulate in the center of the reactor, causing an upward "gulf stream" of polymer powder. Particles closer to the wall are generally moving in a downward direction, thus creating an overall circulation. This intensive (solids) mixing reduces the temperature and concentration gradients in fluid beds, which would affect directly the quality of the polymer produced. However, the rate of mixing in fluid beds is strongly dependent on the scale of operation, see, for example, Matsen (1996).

In the present article, a small-scale FBR is used to study aspects of the polymerization of olefins at conditions resembling those of industrial fluidized-bed reactors as well as widely deviating conditions with controlled thermal gradients. To realize this, the vertical solids mixing, elutriation, and entrainment should be controlled. In the first part of the article, the nonmodified fluidized-bed reactor has been used to study the effect of the fluid dynamics on this small scale. Then, a vertical draft tube has been installed in the center of the fluid bed to control the axial solids mixing. Using the draft tube, the internal solids circulation rate can be controlled by the gas velocity in the draft tube and in the annulus space. In this way, it is possible to simulate the solids circulation pattern observed at an industrial scale in a small-scale unit. Because the draft tube and annulus are generally operated at different gas velocities, both sections have different heat-transport properties, temperatures, and tempera-

Correspondence concerning this article should be addressed to G. Weickert.

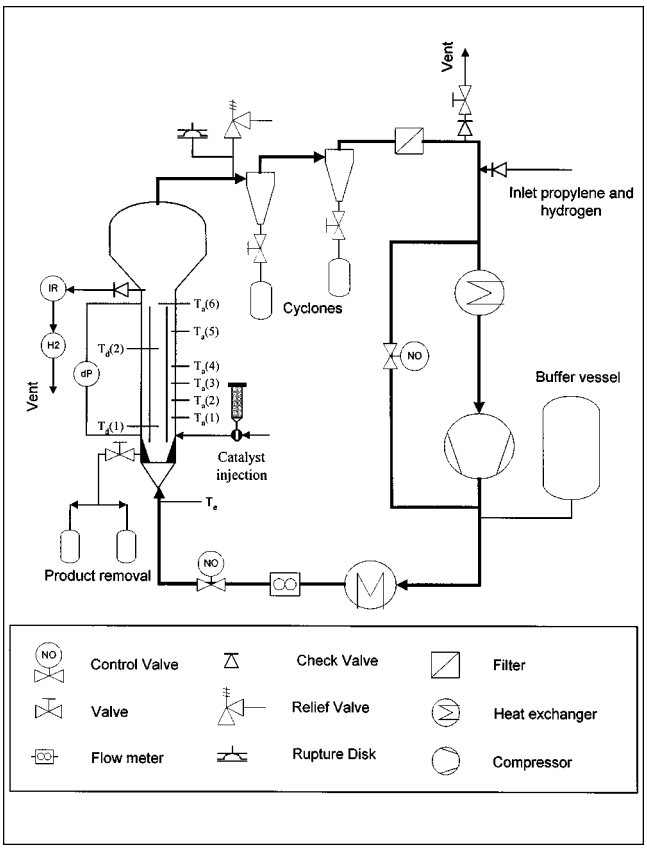

Figure 1. Fluidized-bed reactor.

ture gradients. Therefore, for a particle circulating through the reactor an oscillating particle temperature may occur along the particle trajectory.

Note that a recently developed multizone process for the polymerization of olefins (Montell Technology, 1997) is based on the same principles. Here the solids circulation is based on a riser–downer combination. Although the draft tube can be used to improve the solids mixing, in the present investigation the emphasis is placed on the elimination of segregation and the creation of different zones in one reactor.

Experimental Studies

FBR setup

The experimental setup is shown in Figure 1. The internal diameter and height of the fluid-bed zone is 10 and 100 cm, respectively. The disengagement zone has a diameter of 38.5 cm and a height of 25 cm. Observation ports are available at four different vertical positions (12.5, 37.5, 62.5 and 87.5 cm above the distributor plate). Tracer particles can be injected at a distance of 15 cm above the distributor plate. Polymer samples can be withdrawn at 7 heights ranging from 20 to 80 cm above the distributor at 10 cm intervals. The catalyst is injected 15 cm above the distributor plate (see below). The products can be removed from the bottom section of the reactor, 5 cm above the distributor plate, semicontinuously by opening a valve to the container. The distributor plate consists of sintered stainless-steel spheres with an average pore diameter of 0.3 mm. Steel nuts are packed under the distributor in order to increase mixing and breakup of the inlet velocity profile. Temperatures in the reactor are measured 50 mm below the distributor plate and at six different vertical positions with 10 cm apart, starting at 25 cm above the distributor.

For the experiments with controlled particle mixing, a draft tube and conical bottom section have been installed to force solids circulation with a single gas injection point (see Figure 1). In this setup, particles are forced to move upwards in the draft tube section, and enter the annulus section, where they move in a compact form with no bubbles present under the action of gravity ("moving bed"). Polymer particles leaving the annulus section enter the well-mixed cone section and are reintroduced to the draft tube section. The length, inner diameter, and wall thickness of the draft tube are 770, 50, and 5 mm, respectively. The draft tube, made of glass, is placed in the center of the reactor 130 mm above the distributor plate and is fixed in place by three horizontal rods at the bottom and the top. The inlet diameter and height of the cone are 50 and 150 mm, respectively. Thermocouples in the annulus section are available at six different vertical positions (25, 35, 45, 55, 65, and 90 cm above the distributor plate). Two thermocouples are installed in the draft tube section (20 and 60 cm above the distributor plate). The device for measuring the pressure drop over the annulus is connected to the reactor at 15 and 90 cm above the distributor plate.

Two cyclones and a filter have been installed to remove fines entrained from the reactor. A Eurotherm 900 EPC PID controller controls the temperature of the gas entering the compressor. A heater is used to control the reactor's gas inlet temperature within 0.2°C. The reactor is placed in an air thermostat (50°C) in order to decrease heat losses through the reactor wall to less than 5% of the convective cooling effect by the inlet gas.

The flow circulating through the reactor system is measured by a Brooks mass flow meter. To measure and control the gas composition in the reactor, a sample flow from the reactor is led continuously through a cascaded IR propylene analyzer (Servomex Xendos 2500) and hydrogen analyzer (Maihak, Thermor 615 thermal conductivity meter).

Propylene, hydrogen, and nitrogen are cleaned in separate purification systems to remove traces of O_2, H_2O, CO, and so forth [see Samson et al. (1998)]. Propylene is fed to the system as a liquid just in front of the first heat exchanger. A PID controller controls the partial pressures of propylene and hydrogen. The system is designed to operate at a maximum pressure of 30 bars.

The setup is placed in a concrete bunker and fully computer controlled to determine the temperatures and pressures in the system every 10 s. If a measured value indicates a potentially dangerous situation, catalyst injection is stopped. A relief valve that discharges at 30 bars is placed on top of the reactor. A rupture disk protects the installation for pressures exceeding 32 bars. Combustible-gas detectors are installed to monitor leakage of combustible gas.

Catalyst system

The catalyst used is the well-known metallocene *rac*-$Me_2Si[Ind]_2ZrCl_2$. The catalyst, kindly supplied by Witco Co. Bergkamen (Germany), is supported on PQ silica with a con-

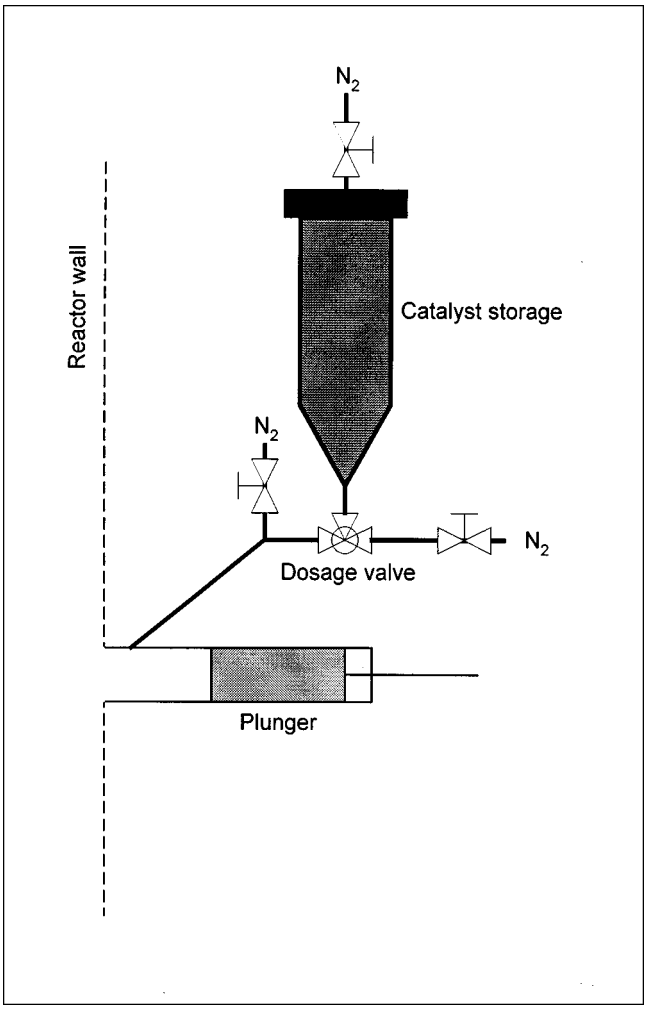

Figure 2. Injection system for catalyst.

centration of 0.79 wt % metallocene. The MAO/SiO_2 support used for immobilization of the metallocene contained 19.1 wt % alumina. Tri-isobutylaluminium (TIBA) has been used as a cocatalyst to increase the catalyst activity. The amount of TIBA and the precontact time was kept constant for all experiments. The exact preparation procedure has been described in a previous article (Meier et al., 2001a).

Catalyst injection system

A semicontinuous system has been developed to inject a small, reproducible amount of catalyst (see Figure 2). The catalyst is diluted with polypropylene powder to prevent the catalyst particles from sticking to each other and to the reactor walls. After connecting the catalyst container to the injection system, all sections are thoroughly flushed with nitrogen. A three-way ball valve, located under the catalyst storage vessel, is used as a dosing device. Shortly before injection, a plunger is displaced, which seals the reactor. To prevent monomer from entering the injection system, a small continuous flow of nitrogen is injected into the reactor when the plunger is pulled back. A small amount of pressurized nitrogen is always kept in the whole injection system to prevent monomer leakage into the injection system. For the semibatch experiments described in this article, the total amount of catalyst is injected within 12 injections at the beginning of the experiment with 20-s intervals between injections.

Electrostatics

To prevent electrostatic charging in the fluidized-bed reactor, the whole setup is electrically grounded. Moreover, Larostat 519 (dimethylethyl ammonium ethosulfate supported on silica, kindly supplied by PPG/Mazer Chemicals) was used as an antistatic agent. The bulk density of the powder is 540 kg/m^3 and the mean particle size is 9 μm. No effect of the antistatic agent on the polymerization rate was found during separate tests in a 0.5-L stirred reactor.

Due to the small average particle size of the powder, some antistatic agent leaves the fluidized-bed reactor zone at high superficial velocities. Addition of a small amount ($\sim$ 200 mg or 0.01 wt %) prior to the catalyst injections assures a sufficient amount of antistatic agent in the reaction zone.

Experimental procedures for mixing and segregation experiments

A LLDPE, Geldart B type powder, kindly supplied by BASF AG (Germany), with a particle size distribution from 100 μm to 1400 μm, was used for mixing and segregation experiments. The average particle size was 900 μm. For the mixing experiments, black tracer particles were prepared from a sieved fraction (420–720 μm) by coloring with black ink. For a mixing experiment, 15–18 g of tracer particles were injected into the FBR. At a specified time interval, samples were taken from the reactor at 7 vertical locations. The tracer concentration was determined using a picture of the sample and counting the colored particles with imaging software. The vertical segregation profile was determined by analyzing the particle-size distribution of samples taken from the bed by laser diffraction (Sympatec Helos LF). The mixing and segregation experiments were executed, with and without an antistatic agent, using nitrogen as the fluidization medium at 25°C.

Experimental procedures for semibatch polymerizations

On startup, the fluidized bed reactor is charged with 1.9 kg of a polypropylene powder, kindly supplied by DSM (The Netherlands). This powder consists of almost ideally spherical particles with a narrow particle-size distribution. The average particle size is 570 μm. Before polymerization can take place, the system must be freed from contamination. This can be done by thoroughly flushing the system with nitrogen and propylene followed by evacuation for 1 h. Propylene is much more effective in cleaning the system than nitrogen. The reason for this is probably that propylene absorbs in the polypropylene under pressure, removing most of the contamination after venting. Before polymerizations are started, 30 g polypropylene precontacted with 0.5 g of TIBA is injected to remove the last traces of impurities.

When the system is at the desired conditions, that is, constant temperature, pressure, fluidization velocity, and gas composition, the system is ready to start the catalyst injections. During the semibatch experiments, a certain amount of

catalyst is injected at the beginning of the experiment. No product is removed from the reaction zone. The amount of polymer produced in each batch experiment is small (less than 300 g compared to 1.9 kg startup powder), which implies a small change in bed height. However, when the draft tube was used, the bed level in the annulus never exceeded the height of the draft tube during the experiment. During the experiments the inlet temperature, fluidization velocity, the total pressure, and partial pressures are kept constant. Because the reactor is to a large degree isolated from the environment, the reaction rate in the semibatch operation can be followed by the temperature response, defined by the nonsteady-state heat balance. The temperature is therefore monitored continuously at the several vertical positions in the reactor. The polypropylene samples obtained at the end of the experiment were characterized with respect to their molecular weight and molecular-weight distribution by Gel Permeation Chromatography (GPC). These GPC measurements were carried out on a Waters M150C apparatus with TSK columns at 140°C using 1,2,4-trichlorobenzene as a solvent.

Experimental procedure for solids circulation measurements with draft tube

On startup, the reactor is charged with 2 kg of polypropylene powder. With this amount of polymer in the system, the bed level in the annulus is about 10 cm below the top of the draft tube. Before the tracer injection, the system is brought to the desired temperature, pressure, gas composition, and gas velocity. About 25 g of colored tracer particles are injected from above at the top of the annulus bed. Because the particles are moving under nearly plug-flow conditions in the annulus, the tracer particles can be watched through the observation ports located at four different vertical positions (12.5, 37.5, 62.5, and 87.5 cm above the distributor plate). The time required for the particles to flow through the annulus section has been used to calculate the circulation rate.

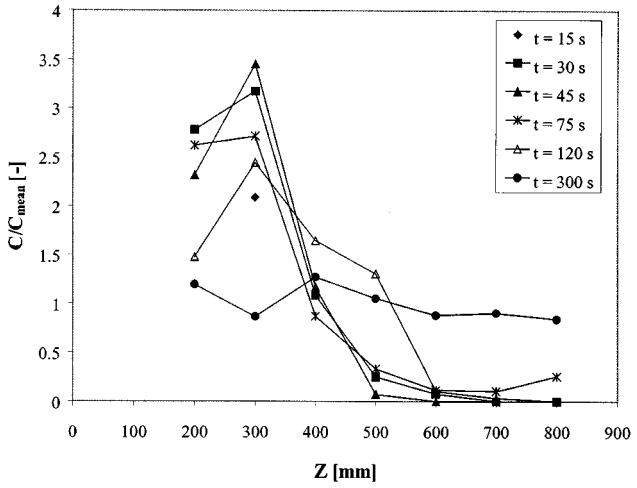

Figure 3. Tracer concentration at different time intervals and vertical position.

Tracer particles injected at $Z = 150$ mm. $U_0 = 11$ cm/s; 26 bar N_2; and 25°C.

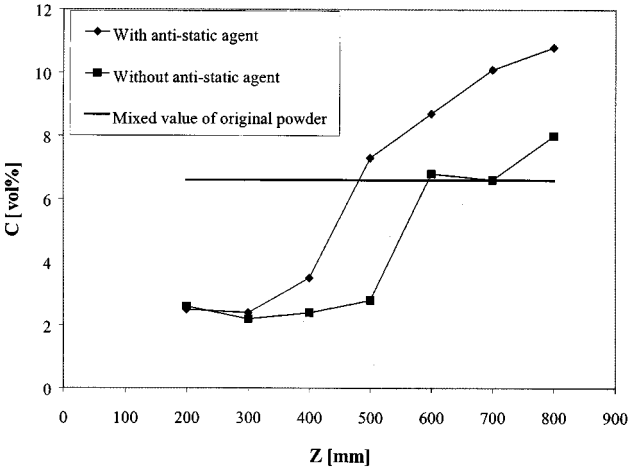

Figure 4. Effect of antistatic agent on the concentration profile of particles $< 420\,\mu$m.

$U_0 = 11$ cm/s, 26 bar N_2, and 25°C.

Results

Mixing of particles without using the draft tube

Using the PE powder at 25°C, the minimum fluidization velocity at 15 bar is 7.5 cm/s, while at 26 bar a value of 6 cm/s has been found. At 15 bar, slugs have been observed in the upper part of the bed, starting at 14 cm/s; at 26 bar, slugs became visible at the slightly higher velocity of 16 cm/s.

Particle mixing has been studied at 11 cm/s and 26 bar nitrogen pressure, which corresponds to 1.8^*U_{mf}. Figure 3 depicts the concentration of the tracer vs. the vertical position in the reactor at different time intervals. The concentration of the tracer has been made dimensionless by division with the mean tracer concentration after a complete mixing. After 15 s, the tracer is only detected at the second sampling point, probably due to upward transport of the tracer during injection with nitrogen. The tracer is mixed up completely after 300 s, which is fast compared to the average residence time for a catalyst particle in a polymerizing system.

Segregation of particles without using the draft tube

The flotsam has been defined as particles smaller than 420 μm. In Figure 4 the segregation pattern can be seen in the absence and presence of the antistatic agent at 11 cm/s and 26 bar, that is, the concentration of flotsam in samples taken at different axial positions before and after injection of the antistatic agent. It can be seen that the concentration of flotsam in the bottom zone of the bed is much lower compared to the concentration in the upper zone. Moreover, injection of the antistatic agent causes an increase in flotsam in the top part of the bed. When no antistatic agent was used, a layer of fines could be observed visually over the length of the reactor wall, obviously caused by electrostatic charging. After an addition of some antistatic agent, the wall deposits disappeared after a few min. The average concentration of particles smaller than 420 μm before the addition of the antistatic agent is smaller than the original value, shown by the horizontal line in Figure 4. After the addition of the antistatic agent, the average concentration equals the average of

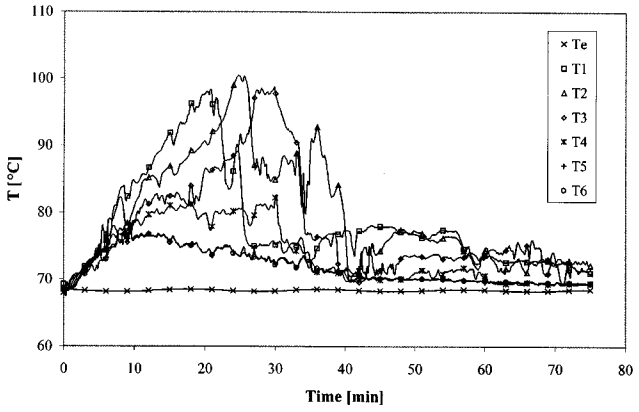

Figure 5. Temperature during an experiment without using the draft tube at 8 cm/s; 1.9*U_{mf}.

the original powder, indicating that no layer is built up any further.

Batch polymerization experiments without using the draft tube

For the batch polymerization experiments a polypropylene powder with almost no fines was used for each experiment (see the experimental section) to minimize the risk of fines sticking at the reactor wall. The polymerizations were done with 65% of propylene, 33% of nitrogen, and 2% of hydrogen at 25 bar and 68.5°C. A minimum fluidization velocity of 4.2 cm/s was found under these conditions. Using air at atmospheric pressure and room temperature, a minimum fluidization velocity of 7.4 cm/s was found.

Three polymerization experiments were executed at three different superficial gas velocities. For each experiment, 0.5 gram of catalyst was used. The development of the vertical temperature profile in time is given in Figures 5, 6 and 7. The superficial velocities were 8, 10, and 13.5 cm/s, respectively. During these experiments, the thermocouple at the highest position, T6, is located above the surface of the bed.

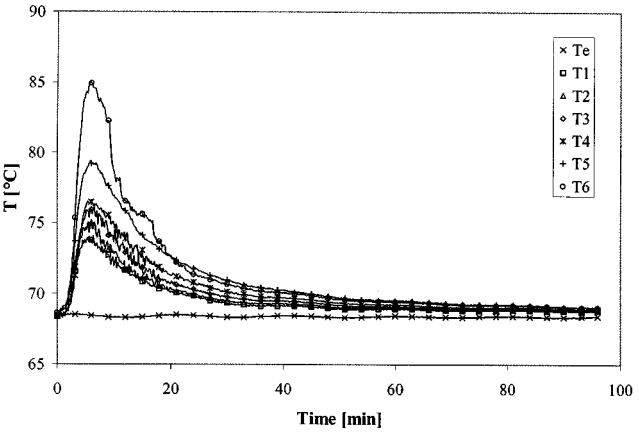

Figure 6. Temperature during an experiment without using the draft tube at 10 cm/s; 2.4*U_{mf}.

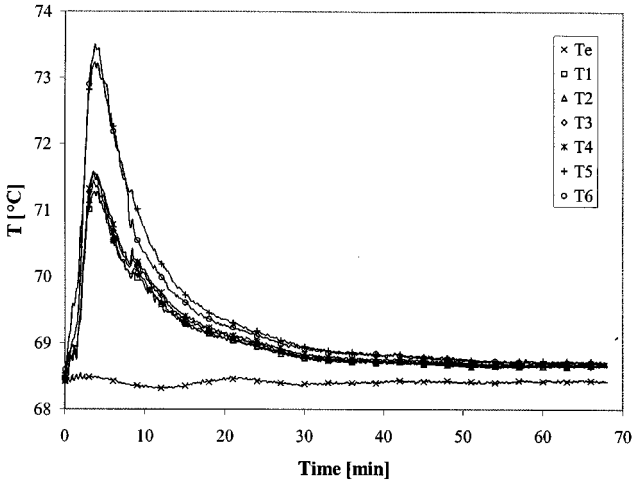

Figure 7. Temperature during an experiment without using the draft tube at 13.5 cm/s; 3.2*U_{mf}.

Increasing U_0 results in a higher convective cooling capacity of the gas, which results in a lower temperature for the reaction zone. When values of U_0-U_{mf} are too low the result is poor mixing behavior of the bed, which may cause local hot spots, agglomeration, and sheeting.

The general behavior just described is confirmed by the experiments presented in Figures 5, 6, and 7, but also see Figure 1. The experiment at 8 cm/s, 1.9*U_{mf}, shows a very diffuse temperature profile. Due to the low value of U_0-U_{mf}, mixing in the bed is limited and local hot spots are observed. It is remarkable that even with a low-activity catalyst, as used in the present work, high local temperatures can exist. At the beginning of the experiment the highest temperature was observed in the bottom section of the reactor. It seems that a hot front slowly moves upwards to the top of the bed. This can be explained by a slowly segregating bed where the high catalyst concentration zone moves to the top of the bed.

The mixing experiment described earlier, carried out by the tracer injection, showed a relatively fast mixing behavior. This seems to contradict the result of the batch polymerization experiment. There are several reasons for the reduced mixing under reaction conditions. First, it has to be mentioned that the mixing experiments were carried out with a different particle-size distribution. Moreover, the mixing experiments were carried out using nitrogen as fluidization gas. During the polymerization experiments, propylene is sorbed by the amorphous phase of the polypropylene, which causes swelling of the polymer. The molecular weight of the polypropylene produced with the applied metallocene catalyst system is very low; about 20 kg/mol. This polymer is sticky under reaction conditions, and is probably the major source of the limited mobility in the bed.

The experiment at 10 cm/s, 2.4*U_{mf} (see Figure 6), shows a regular temperature pattern with a lower maximum temperature and some temperature gradients inside the bed. The lowest temperature was found in the bottom section of the bed, as expected. The two thermocouples, T5 and T6, measure a significantly higher temperature than the thermocouples in the bed, indicating relatively high polymerization ac-

tivity in the top section of the bed and the lean phase above the bed.

The experiment at 13.5 cm/s, 3.2*U_{mf} (see Figure 7), shows the lowest maximum temperature and lowest temperature gradients in the bed. The two thermocouples, T5 and T6, again measure a significantly higher temperature than the thermocouples in the bed. It appears that the upper zone of the bed has a high catalyst concentration due to segregation of the catalyst. The elutriation of fine particles didn't result in entrainment of particles from the reactor, because no material, except from some antistatic agent, was found in the cyclones.

It is obvious that the observed problems with mixing and segregation are related to the small scale of the reactor. In our small-scale FBR the average bubble size is about half of the reactor diameter. This ratio is quite different in an industrial-size reactor. Here the reactor diameter and height are about 4 and 12 m, respectively. Moreover, the mixing of solids is determined by the macroscale circulation pattern of solids generally observed in reactors of this scale. The bubbles tend to accumulate in the center of the reactor, causing an upward "gulf stream" of solids in the center and downflow near the reactor wall. These phenomena are not observed in reactors at a small-scale, as used in the present study.

To overcome the problems observed, a draft tube was installed in the reactor, which allows us to control the solids mixing in the reactor.

Solids circulation using the draft tube

Experiments at different pressures and gas compositions have been executed (see Table 1), to study the influence on the circulation rate. The residence time of solids in the annulus section has been measured as a function of the gas velocity (see Figure 8). Note that the gas velocity is based on the velocity at the cone inlet, that is, 50 mm in diameter. This velocity does not represent the fluidization velocity in the draft tube or annulus section, as the gas is divided over these two sections. As can be seen from Figure 8, the residence time of the solids in the annulus decreases with increasing gas velocity. The gas density hardly influences the circulation rate, although some differences have been observed between the experiments at 15 and 25 bar with 65% propylene. The measured solids velocity in the annulus remains the same for all experiments (between 1.7 and 3.5 cm/s) below the minimum fluidization velocity, that is, 4.2 cm/s.

A certain minimum gas velocity ($U_{e,\min}$) is required to start the circulation of solids in the system. This minimum gas velocity decreases with the increasing density of the gas phase. The minimum gas velocity required at atmospheric pressure is about 42 cm/s, whereas this velocity is about 24 cm/s at 25 bar with 65% propylene.

Table 1. Process Conditions for Circulation-Rate Measurements

T (°C)	p (bar)	Propylene (%)	Nitrogen (%)	ρ_g (kg/m^3)
338	25	65	35	35.5
338	25	0	100	25.0
338	15	65	35	20.4
293	1		Air	1.0

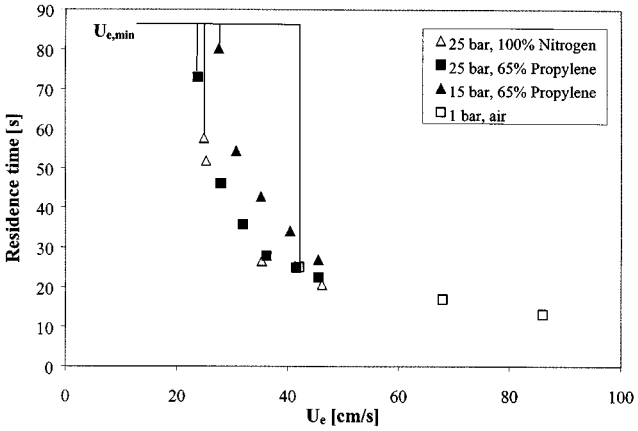

Figure 8. Solids residence time in the annulus with a length of 77 cm as a function of gas velocity.

$U_{e,\min}$ represents the minimum gas velocity to start solids circulation.

Further visual observation of the solids circulation experiments showed that the tracer particles were mixed through the reactor contents after 3 to 4 circulations, that is, 1–5 minutes, depending on the circulation rate. Most of the mixing is achieved in the cone section. The flow behavior of solids in the draft tube is of the slugging type. At very high velocities, 45 cm/s, a transition toward turbulent fluidization is observed. Only minor dispersion of solids in the annulus is observed. No bubbles in the annulus section have been detected.

The pressure drop over the annulus has been measured at different gas velocities and bed weights using nitrogen at 25 bar and 60°C as the fluidization medium (see Figure 9). As expected, larger pressure drops with increasing bed weight have been observed. Increasing the gas velocity results in a decreasing pressure drop over the annulus, indicating a lower solids holdup in the draft tube with increasing gas velocity because of the coupled pressure balance for the annulus and draft tube. The bed height in the annulus is almost constant with increasing gas velocity. The decreasing pressure drop

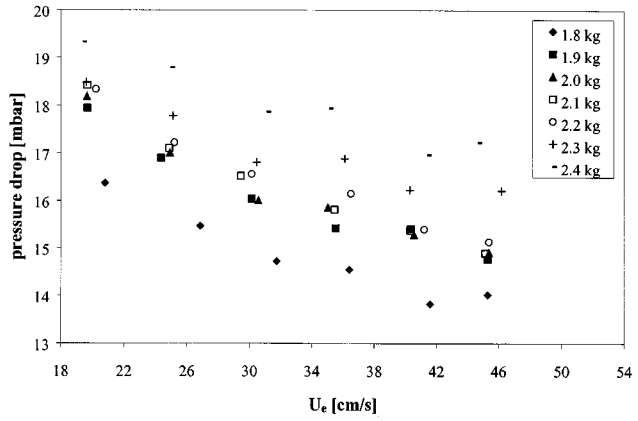

Figure 9. Influence of total polymer holdup on the pressure drop over the annulus as a function of the gas velocity using 25 bar N_2 at 60°C.

over the system with increasing gas velocity also indicates a decreasing upward gas velocity in the annulus section with increasing gas velocity. The reduced amount of gas bypassing to the annulus with increasing gas velocity is in agreement with the results reported by Ji et al. (1998).

The Ergun equation was used to calculate the minimum upward gas velocity in the annulus, that is, at the highest solids circulation rate. Assuming a bed porosity of 0.42 and a shape factor of 1, a slip velocity of 4.6 cm/s was found. The downward solids velocity at these conditions is 3.5 cm/s. The minimum upward gas velocity in the annulus is therefore 1.1 cm/s.

Semibatch polymerizations using the draft tube

Semibatch propylene polymerizations were executed at 25 bar and different gas velocities, that is, different solids circulation rates. The first experiment was executed with a gas inlet temperature of 68°C. Before the catalyst is injected the system is stabilized, that is, constant temperature, pressure, gas velocity, and so on. Then the total amount of catalyst is injected in about 4 min. The responding temperature behavior of the semi-isolated fluid bed will have the shape of a broad pulse, because the catalyst is subject to deactivation. Only at a very high solids circulation rate, both in the draft tube and annulus, would all thermocouples indicate the same temperature. At lower circulation rates temperature gradients will appear in both sections as follows. Particles coming from the annulus will be cooled down in the cone by the relative cold gas, thereby absorbing monomer. On the way up in the draft tube, the temperature will increase a little due to the polymerization reaction, although this remains a small effect due to the short residence time in this section. Along the way down in the annulus, much more polymerization takes place at these longer residence times and less convective cooling capacity is available, resulting in a relatively large temperature gradient.

The temperature profile of the annulus section of the first experiment is presented in Figure 10. The initial decrease in temperature is due to the catalyst injections with cold nitrogen. After the catalyst injections, the temperature starts rising rapidly and reaches a maximum after about 15 min. At this point, the largest temperature gradients inside the reactor—about 5°C—have been observed. Note that in contrast to the reactor without a draft tube, the highest temperatures are now found in the bottom of the reactor. Then the catalyst starts to deactivate and the temperature inside the reactor returns to its initial value after about 1.5 h. The maximum temperature observed in this experiment was about 83°C. In a recently published article (Meier et al., 2001a), strongly reduced yields were found at temperatures above 80°C using the same catalyst system.

Table 2. Process Conditions for Polymerization Experiments Using Draft Tube (T_e = 58°C)

U_e (cm/s)	$u_{a,s}$ (cm/s)	$[C_3H_6]$ (%)	$[N_2]$ (%)	$[H_2]$ (%)
25.1	1.7	69.6	29.4	1.0
30.4	2.3	69.0	30.0	1.0
36.2	3.0	66.6	32.4	1.0
42.7	3.5	67.1	31.9	1.0

The next series of experiments were therefore executed with a gas inlet temperature of 58°C (see Table 2). The temperature profiles of the annulus section of these experiments are given in Figures 11–14. The experiment at the lowest gas velocity, 25.1 cm/s, shows the highest internal temperature gradient and absolute temperature. The experiment at 42.7 cm/s shows only minor internal temperature gradients of about 1°C, and may be interpreted as an experiment in a CSTR. The scattering at 30.4 cm/s during the initial phase of the experiment and twice at 36.2 cm/s during the experiment is due to some solids circulation disturbances, probably due to some temporary sticking of particles at the thermocouples.

The temperature gradients measured inside the draft tube section are due much less to the high gas velocity. The gas velocity in the draft tube is for the experiments at 25.1 and 42.7 cm/s, about 3.3 and 7.6 times U_{mf}, respectively. The temperature gradients in the draft tube observed for the experiment at the highest and lowest circulation rates were 0.2 and 1°C, respectively.

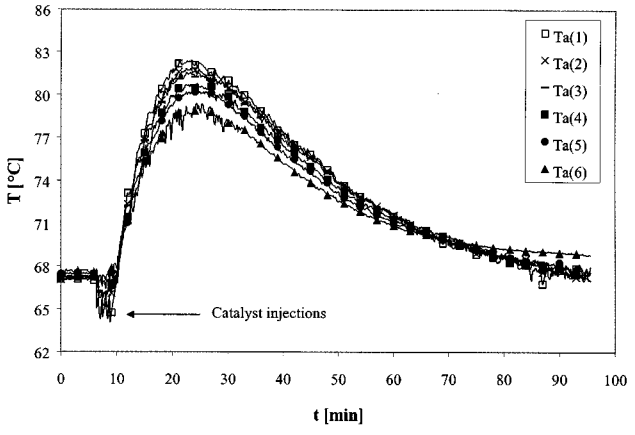

Figure 10. Temperature of the annulus as a function of time during a semibatch polymerization.

Ta(1) and Ta(6) indicate the temperature in the bottom and top of the annulus, respectively.

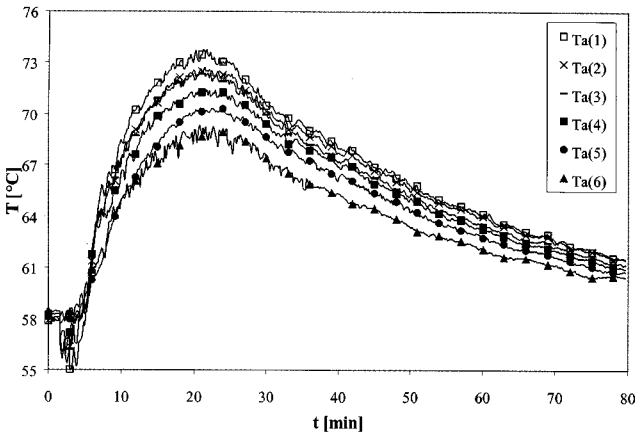

Figure 11. Temperature of the annulus as a function of time during a semibatch polymerization.

U_e = 25.1 cm/s, $u_{a,s}$ = 1.7 cm/s.

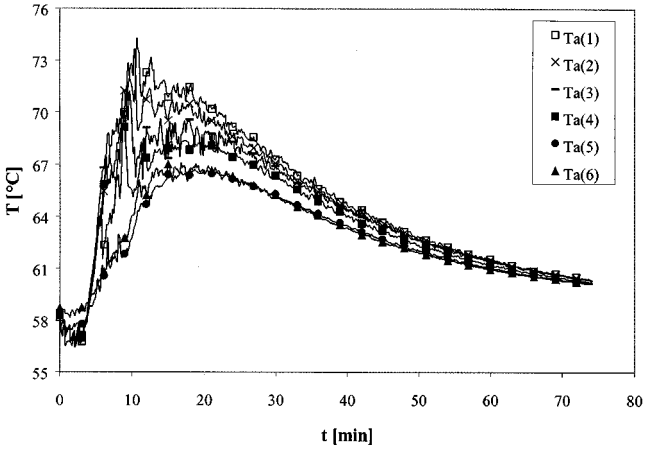

Figure 12. Temperature of the annulus as a function of time during a semibatch polymerization.

U_e = 30.4 cm/s, $u_{a,s}$ = 2.3 cm/s.

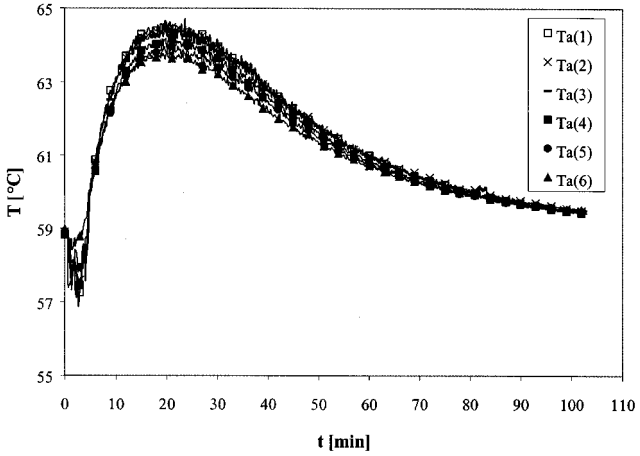

Figure 14. Temperature profile of the annulus as a function of time during a semibatch polymerization.

U_e = 42.7 cm/s, $u_{a,s}$ = 3.5 cm/s.

Injection of hydrogen

From kinetic experiments previously published (Meier et al., 2001a), it was concluded that the current catalyst system is sensitive to hydrogen. The molecular weight of the polymer produced decreases with increasing hydrogen concentration, whereas the polymerization activity increases with increasing hydrogen concentration. The main reason for the increased polymerization rate is that hydrogen prevents the formation of dormant sites, which occur after a secondary insertion of propylene.

In the next series of experiments (see Figure 15), hydrogen was injected in the gas recycle at different moments during semibatch experiments. Thus a certain fraction of the end product is produced at a low hydrogen concentration, yielding a high molecular-weight polymer, while the other part of the product is produced at a high hydrogen concentration, which yields a low molecular-weight polymer. During the experiment the propylene concentration is kept at its initial value—60 vol %—that is, the pressure increases about 1 bar after the injection of hydrogen. The hydrogen concentration before the injection is 0.0217 kg/m^3 (~ 1 vol %), while after the hydrogen injection the concentration is raised to 0.123 kg/m^3 (7 vol %). All experiments have been executed with a gas inlet temperature of 59.5°C and a gas velocity of 36 cm/s, that is, about 3 cm/s solids velocity in the annulus.

Figure 15 depicts the results of the hydrogen pulse experiments, showing the difference between the gas inlet temperature and the temperature at the bottom of the annulus, $T_a(1)$, during the experiments. The negative value of $T_a(1)$-T_e during the first couple of minutes is the result of the catalyst being injected with cold nitrogen. As can be seen from Figure 15, the temperature immediately increases after an injection of hydrogen, indicating an almost instantaneous increase in

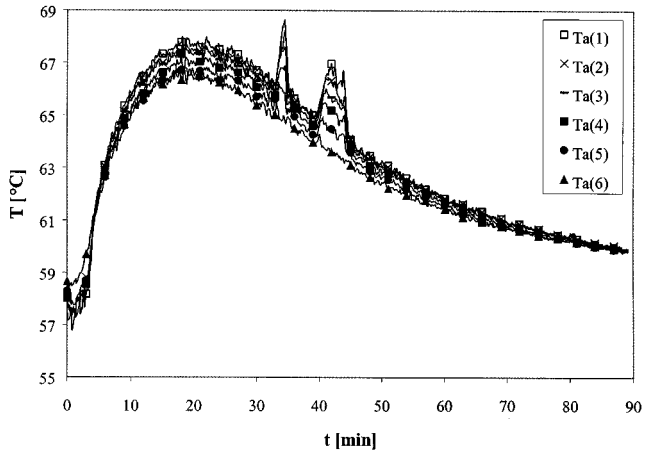

Figure 13. Temperature profile of the annulus as a function of time during a semibatch polymerization.

U_e = 36.2 cm/s, $u_{a,s}$ = 3.0 cm/s.

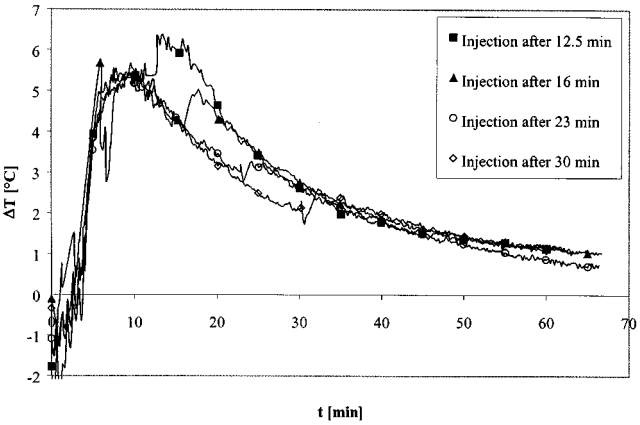

Figure 15. Temperature difference between the bottom of the annulus and reactor inlet during different semibatch polymerizations with hydrogen injections at different moments.

U_e = 36 cm/s, $u_{a,s}$ = 3 cm/s.

the polymerization rate. The reaction rate to reactivate the dormant sites is probably fast.

A second feature observed in Figure 15 is that the different temperature curves follow more or less the same master curve before and after the injection of hydrogen. The active sites probably deactivate at about the same rate at the applied process conditions. Moreover, the relative increase in temperature after the injection is more or less constant. Because the increase is probably caused by the reactivation of dormant sites, one may conclude that the relative concentration of dormant sites, relative to the number of active sites, is constant during the experiment. Dormant sites probably deactivate at the same rate as the active sites.

Reactor Model

A large number of publications have appeared in the literature dealing with the mathematical modeling of the phenomena taking place in conventional fluidized-bed reactors for olefin polymerization (for example, Choi and Ray, 1985; Talbot, 1990; McAuley et al., 1994). None of them have been verified by experimental data, see also Matsen (1996) for scaling-up problems.

In this article, a reactor model has been developed based on the actual gas and solid flow, which should be able to describe the temperature and concentration gradients inside the reactor and the related molecular-weight distribution of the polymer product. The reactor model uses the measured solids circulation-rate measurements as input. The results of the circulation-rate measurements are closely related to the geometry of the setup, for example, diameter and length of the draft tube, the distance between draft tube and cone, and the angle of the cone. Several authors have reported that the geometry of the reactor has a large influence on the solids circulation rate (for example, Ji et al., 1998; Alappat and Rane, 1995; Song et al., 1997; Berruti et al., 1988; Yang and Keairns, 1983). No data are available on pressurized systems. In the present article at the given geometry, only the influence of the gas velocity on the solids circulation rate has been investigated and is used as input for the model.

The assumptions for the reactor model are summarized below.

(1) The reactor is divided into three sections; the annulus, draft tube, and cone sections. The draft tube and annulus sections are divided in N CSTRs in series to simulate plug-flow regimes in both sections. The cone is considered as one CSTR. The reactor model is presented in Figure 16.

(2) The resistance to mass and heat transfer between the gas and solids in each compartment is negligible, which is acceptable (Floyd et al., 1986) in the case where the catalyst activity is not extremely high and the particles are relatively small. Particles circulating in the system are continuously absorbing and desorbing propylene due to the temperature gradients in the system. Equilibrium is assumed in each compartment.

(3) The energy effects due to absorption and desorption of propylene have been neglected.

(4) The gas and solids velocities in the reactor are assumed to be constant, because the monomer conversion per pass through the reactor is low.

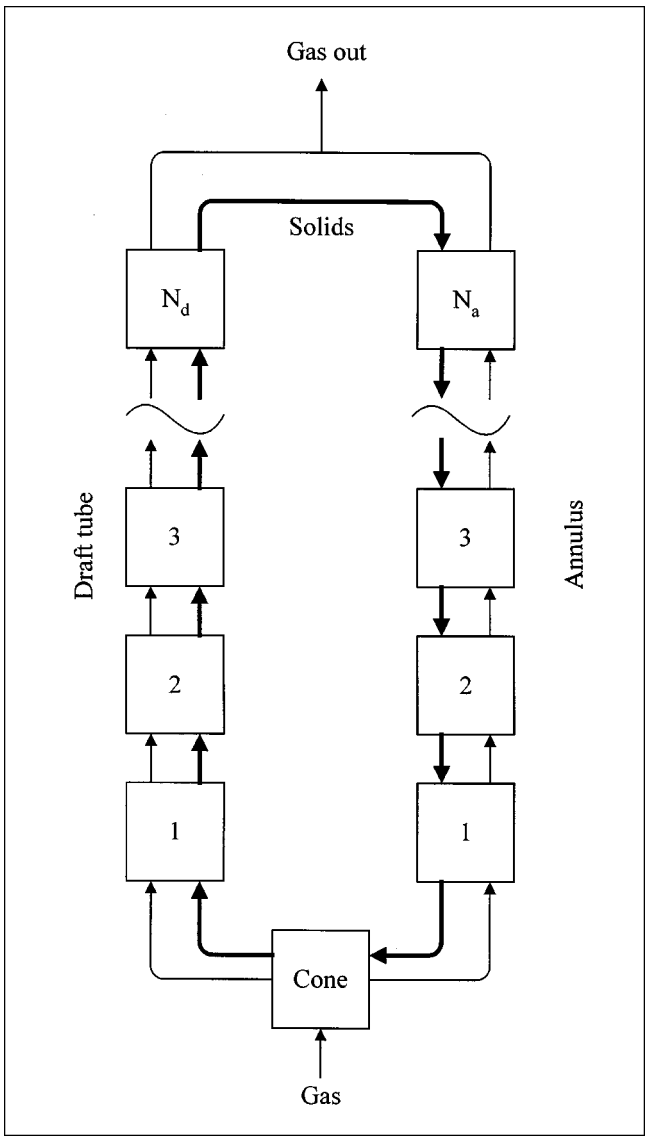

Figure 16. Reactor model.

(5) Minimum fluidization conditions for the annulus have been assumed. The voidage of the cone and draft tube sections is equal to the experimentally determined value.

(6) No heat transfer from the annulus to the draft tube section takes place.

(7) The heat transfer from the annulus bed to the reactor wall combined with the heat transfer through the wall is relatively fast compared to the heat transfer from the reactor wall to the reactor surroundings. This is so because the reactor is placed in an air thermostat at 50°C, which reduces the heat losses to a large extent. It is assumed that the wall temperature of the adjacent annulus compartment equals the temperature of the reactor contents. Heat losses are described using a Nusselt correlation for heat transfer from a flat plate to laminar flowing air.

The kinetic model and kinetic constants are based on an experimental study (Meier et al., 2001a) using the same cata-

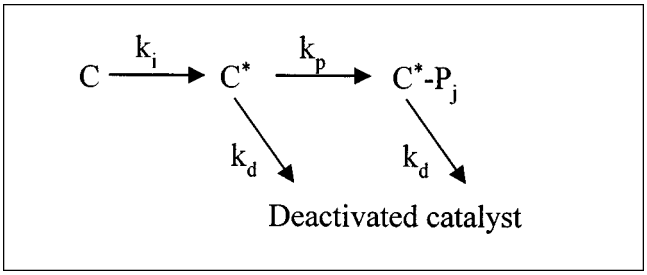

lyst system. The model does respect the initiation and deactivation of the catalyst, see Scheme 1. The reaction rate is described by first-order kinetics with respect to the number of active sites, C^*, and the monomer concentration in the polymer, C_m. The monomer concentration is calculated using the Flory–Huggins equation. The Flory–Huggins interaction parameter is based on experimental data published previously (Meier et al., 2001b). The density and heat capacity of the gas phase are functions of the local temperature and gas composition, and have been described according to Peng-Robinson and Daubert et al. (1985), respectively.

To obtain a clear understanding of the reactor model, the material and energy balances will be described separately for the cone compartment, an arbitrary draft tube, and annulus compartment (see Figure 16).

Cone compartment

Mass balance for nonactivated catalyst in the cone

$$\frac{dC_c}{dt} = \phi_{m,s}\left(X_{a,1}^C - X_c^C\right) - k_i C_c \tag{1}$$

Here X_c^C is the mass fraction of nonactivated catalyst in the cone, defined as

$$X_c^C = \frac{C_c}{C_c + V_c(1-\epsilon_c)\rho_s} \tag{2}$$

The first term on the right side of Eq. 1 concerns the convective flow of nonactivated catalyst. The second term concerns the initiation of nonactivated catalyst with initiation rate constant, k_i.

Mass balance for activated catalyst in the cone

$$\frac{dC_c^*}{dt} = \phi_{m,s}\left(X_{a,1}^{C^*} - X_c^{C^*}\right) + k_i C_c - k_d C_c^* \tag{3}$$

Here $X_c^{C^*}$ is the mass fraction of activated catalyst in the cone, defined as

$$X_c^{C^*} = \frac{C_c^*}{C_c^* + V_c(1-\epsilon_c)\rho_s} \tag{4}$$

The first term on the right side of Eq. 3 concerns the flow of activated catalyst. The second term is the initiation toward active catalyst, and the third term concerns the deactivation of the catalyst.

Mass balance for monomer in the cone

$$\frac{d\left(V_c \epsilon_c \rho_g m_c^m\right)}{dt} = U_e A_e \rho_g \left(m_e^m - m_c^m\right) - R_{p,c} \tag{5}$$

The first term on the right side of Eq. 5 concerns the flow of monomer through the cone. The second term represents the consumption of monomer in the cone due to polymerization.

The reaction rate in the cone compartment is described by

$$R_{p,c} = k_p C_c^* C_{m,c} \tag{6}$$

Here C_c^* stands for the amount of activated catalyst in the cone compartment.

Energy balance for the cone

$$\frac{d\left(V_c \rho_{av,c} C_{p,av,c} T_c\right)}{dt} = U_e A_e \rho_g C_{p,g}(T_e - T_c) + \phi_{m,s} C_{p,s}(T_{a,1} - T_c) + R_{p,c}\Delta H_r \tag{7}$$

The first two terms on the right side of Eq. 7 concern the enthalpy associated with the gas and solid flow through the cone. The third term stands for the amount of heat produced due to polymerization.

Starting conditions for the cone at $t = 0$

$$\begin{aligned} C_c(0) &= C_{c,0} \\ C_c^*(0) &= 0 \\ T_c(0) &= T_0 \\ m_c^m(0) &= m_0^m \end{aligned} \tag{8}$$

Draft tube compartment i

The mass and energy balances for a draft tube compartment are analogous.

Mass balance for nonactivated catalyst

$$\frac{dC_{d,i}}{dt} = \phi_{m,s}\left(X_{d,i-1}^C - X_{d,i}^C\right) - k_i C_{d,i} \tag{9}$$

Here $X_{d,i}^C$ is the mass fraction of nonactivated catalyst, defined as

$$X_{d,i}^C = \frac{C_{d,i}}{C_{d,i} + V_{d,i}(1-\epsilon_d)\rho_s} \tag{10}$$

Mass balance for activated catalyst

$$\frac{dC_{d,i}^*}{dt} = \phi_{m,s}\left(X_{d,i-1}^{C^*} - X_{d,i}^{C^*}\right) + k_i C_{d,i} - k_d C_{d,i}^* \tag{11}$$

Here $X_{d,i}^{C^*}$ is the mass fraction of activated catalyst, defined as

$$X_{d,i}^{C^*} = \frac{C_{d,i}^*}{C_{d,i}^* + V_{d,i}(1-\epsilon_d)\rho_s} \tag{12}$$

Mass balance for monomer

$$\frac{d\left(V_{d,i}\,\epsilon_d\,\rho_g\,m^m_{d,i}\right)}{dt} = u_{d,g}\,A_d\,\rho_g\left(m^m_{d,i-1} - m^m_{d,i}\right) - R_{p,d,i} \quad (13)$$

The equation for the polymerization rate

$$R_{p,di} = k_p C^*_{d,i} C_{m,d,i} \quad (14)$$

Energy balance

$$\frac{d\left(V_{d,i}\,\rho^{av}_{d,i} C^{av}_{p,d,i} T_{d,i}\right)}{dt} = u_{d,g}\,A_d\,\rho_g C_{p,g}\left(T_{d,i-1} - T_{d,i}\right) + \phi_{m,s} C_{p,s}\left(T_{d,i-1} - T_{d,i}\right) + R_{p,d,i}\Delta H_r \quad (15)$$

Starting conditions for $t = 0$

$$\begin{aligned} C_{c,i}(0) &= C_{d,0} \\ C^*_{d,i}(0) &= 0 \\ T_{d,i}(0) &= T_0 \\ m^m_{d,i}(0) &= m^m_0 \end{aligned} \quad (16)$$

Coupling between cone and draft tube

$$\begin{aligned} T_{d,0} &= T_c \\ X^C_{d,0} &= X^C_c \\ X^{C^*}_{d,0} &= X^{C^*}_c \\ m^m_{d,0} &= m^m_c \end{aligned} \quad (17)$$

Annulus compartment i

Mass balance for nonactivated catalyst

$$\frac{dC_{a,i}}{dt} = \phi_{m,s}\left(X^C_{a,i+1} - X^C_{a,i}\right) - k_i C_{a,i} \quad (18)$$

Here $X^C_{a,i}$ is the mass fraction of nonactivated catalyst, defined as

$$X^C_{a,i} = \frac{C_{a,i}}{C_{a,i} + V_{a,i}(1-\epsilon_a)\rho_s} \quad (19)$$

Mass balance for activated catalyst

$$\frac{dC^*_{a,i}}{dt} = \phi_{m,s}\left(X^{C^*}_{a,i+1} - X^{C^*}_{a,i}\right) + k_i C_{a,i} - k_d C^*_{a,i} \quad (20)$$

Here $X^{C^*}_{a,i}$ is the mass fraction of activated catalyst, defined as

$$X^{C^*}_{a,i} = \frac{C^*_{a,i}}{C^*_{a,i} + V_{a,i}(1-\epsilon_a)\rho_s}. \quad (21)$$

Mass balance for monomer

$$\frac{d\left(V_{a,i}\,\epsilon_a\,\rho_g\,m^m_{a,i}\right)}{dt} = u_{a,g}\,A_a\,\rho_g\left(m^m_{a,i-1} - m^m_{a,i}\right) - R_{p,a,i} \quad (22)$$

The equation for the polymerization rate

$$R_{p,ai} = k_p C^*_{a,i} C_{m,a,i} \quad (23)$$

Energy balance

$$\frac{d\left(V_{a,w,i}\,\rho^{av}_{a,i} C^{av}_{p,a,i} T_{a,i}\right)}{dt} = u_{a,g}\,A_a\,\rho_g C_{p,g}\left(T_{a,i-1} - T_{a,i}\right) + \phi_{m,s} C_{p,s}\left(T_{a,i+1} - T_{a,i}\right) + R_{p,a,i}\Delta H_r - \alpha_{a,i}\frac{1}{4}\pi D_r^2\left(T_{a,i} - T_\infty\right) \quad (24)$$

Because the heating and cooling of the reactor wall is included in the accumulation term, the density and heat capacity of the annulus compartment is based on the weight-averaged value of the gas, solids, and the stainless-steel wall. The last term in Eq. 24 concerns the heat transfer from the reactor wall to the air flowing through the isolated metal cage.

Starting conditions for $t = 0$

$$\begin{aligned} C_{a,i}(0) &= C_{a,0} \\ C^*_{a,i}(0) &= 0 \\ T_{a,i}(0) &= T_0 \\ m^m_{a,i}(0) &= m^m_0 \end{aligned} \quad (25)$$

Coupling between cone and draft tube and annulus

$$\begin{aligned} T_{a,0} &= T_c \\ T_{a,N_a+1} &= T_{d,N_d} \\ X^C_{a,N_a+1} &= X^C_{d,N_d} \\ X^{C^*}_{a,N_a+1} &= X^{C^*}_{d,N_d} \\ m^m_{a,0} &= m^m_c \end{aligned} \quad (26)$$

Sensitivity to hydrogen

Both the propagation rate constant and the initiation rate constant depend on the concentration of hydrogen in the gas phase [see Meier et al. (2001a)]. It was found that the deactivation rate constant was not sensitive to hydrogen above hydrogen concentrations of 0.01 kg/m^3. The sensitivity to hydrogen of both k_p and k_i is described as empirical relations (see Eqs. 27 and 28)

$$k_p = \left(a_p[H_2]^c + b_p\right)e^{E_{\mathrm{act},p}/RT} \quad (27)$$

$$k_i = \left(a_i[H_2] + b_i\right)e^{E_{\mathrm{act},i}/RT} \quad (28)$$

$$k_d = k_{d,o}\,e^{E_{\mathrm{act},d}/RT} \quad (29)$$

Table 3. Input Data for Reactor Model

Constant	Value	Unit	Constant	Value
a_p	1.8×10^{7}	$m^3/[kg\cdot s\cdot(kg/m^3)^c]$	$E_{act,p}$	43.9 kJ/mol
a_i	9.72×10^{4}	$m^3/kg\cdot s$	ΔH_r	2471 kJ/kg
A_e	1.96×10^{-3}	m^2	k_{d0}	0.36 L/s
A_a	5.03×10^{-3}	m^2	N_a	20 —
A_d	1.96×10^{-3}	m^2	N_d	20 —
b_p	2.27×10^{6}	$m^3/kg\cdot s$	T_∞	50°C
b_i	1.07×10^{3}	L/s	ϵ_a	0.44 —
c	0.3	—	ϵ_c	0.75 —
d_w	4×10^{-2}	m	ϵ_d	0.75 —
$E_{act,d}$	17.4	kJ/mol	ρ_s	910 kg/m^3
$E_{act,I}$	35.6	kJ/mol		

Molecular-weight distribution

The molecular-weight distribution of the product from a single-site catalyst can in general be described with a Schulz–Flory distribution. It was shown in a previous article (Meier et al., 2001a) that the molecular-weight distribution of the polymer produced with the current heterogeneous metallocene catalyst can best be described with a "two-site model." The chain transfer probability of sites 1 and 2 depends only on the hydrogen concentration divided by the monomer concentration (in the polymer).

At constant temperature, pressure, and gas composition, the instantaneous molecular-weight distribution of a polymer synthesized with a single-site catalyst can be described with a Schulz–Flory distribution (see Eq. 30)

$$y_j^d = jq^2e^{-jq} \tag{30}$$

Here, y_j^d is the density function of the instantaneously formed molecular-weight distribution. The "two-site model" presented in a previous article (Meier et al., 2001a) uses two Schulz–Flory distributions, equal polymerization rate for each site, but with a different chain termination probability, q. The chain transfer probability of sites 1 and 2 depends only on the relative hydrogen concentration (see Eqs. 31 and 32). The monomer concentration in the polymer, C_m, depends on the temperature

$$q_1 = 3.027\frac{C_{H_2}}{C_m} + 0.0023 \tag{31}$$

$$q_2 = 14.31\frac{C_{H_2}}{C_m} + 0.0051 \tag{32}$$

The molecular-weight distribution of the polymer product obtained after the polymerization experiment in the internally circulating fluidized-bed reactor can be calculated by integration over time and place in the reactor. For our reactor model, we can summarize the molecular-weight distributions produced during an integration interval for every compartment, based on the amount of polymer produced in that time interval.

The related weight- and number-averaged molecular-weight of the polymer can be calculated by the moments of distribution

$$N_n = \sum_{j=1}^{\infty} M_{w,j}^{n-1} y_j^d \tag{33}$$

$$M_w = \frac{N_2}{N_1}, \quad M_n = \frac{N_1}{N_0} \tag{34}$$

Modeling Results

The number of mixing cells in the annulus and draft tube (N_a and N_d) remain to be determined or fixed. It was found from preliminary calculations that 20 compartments in the annulus and draft tube were sufficient ($N_a = N_d = 20$) to simulate the plug flow behavior in these two sections. Increasing the number of compartments in these two sections does not affect the predicted results. Other input data are summarized in Table 3. The system of differential equations (164 in all) is numerically solved by the Runge–Kutta method. In Figures 17 and 18 the model prediction of the temperature profile in the annulus, together with the results of the experiments at 25.1 and 42.7 cm/s, are presented. The shapes of the temperature curves are comparable with the experimental results. It seems that the deactivation rate of the catalyst is overpre-

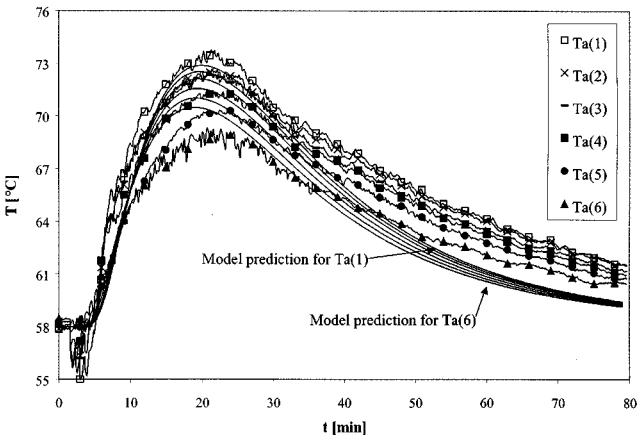

Figure 17. Experimental result vs. model prediction for the experiment at 25.1 cm/s.

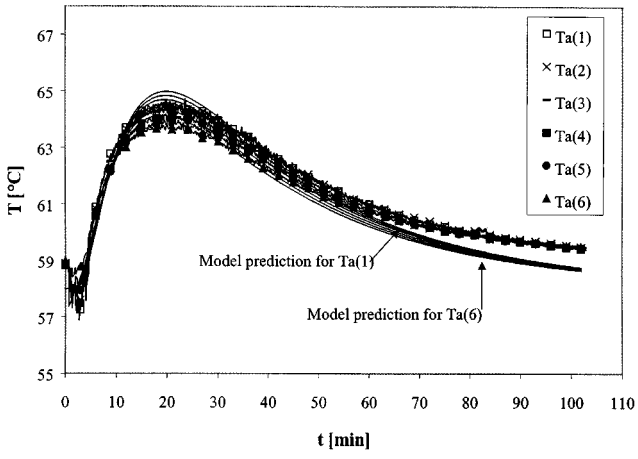

Figure 18. Experimental result vs. model prediction for the experiment at 42.7 cm/s.

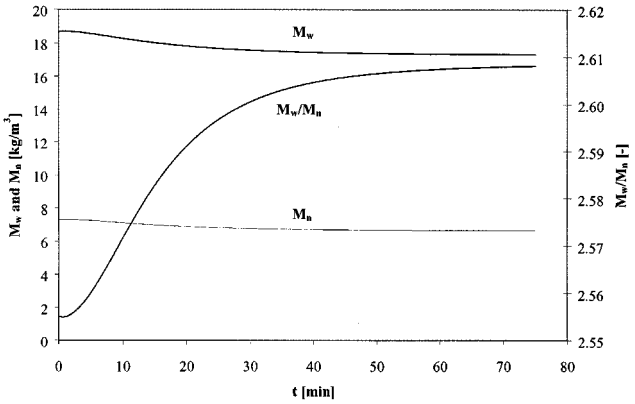

Figure 19. Model prediction of the weight and number-averaged molecular weight and polydispersity as a function of time during the experiment at 25.1 cm/s.

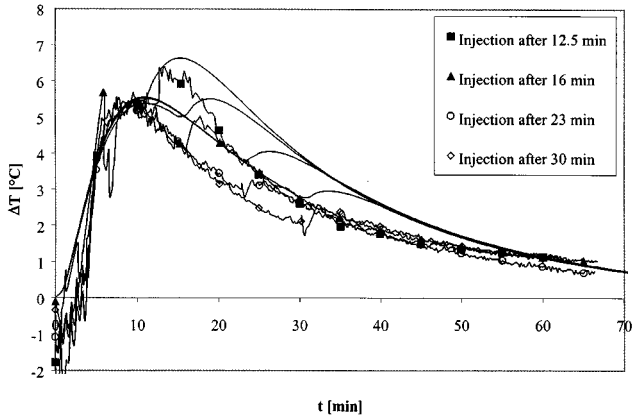

Figure 20. Experimental results vs. model predictions for the experiments with injections of hydrogen.

dicted by the model, leading to an underprediction of the temperature at the end of the experiment. The temperature gradient over the length of the annulus is somewhat underpredicted. This can be explained as follows. The model uses the solids circulation measurements described earlier in this article as input data. These measurements were carried out under nonpolymerization conditions with the same polymer powder as was used as a startup powder for the polymerization experiments. However, during the polymerization experiments a low molecular-weight polymer was formed that was somewhat sticky. This may cause reduced mobility of the polymer powder inside the reactor, and lead to reduced circulation rates and higher internal temperature gradients than expected. Furthermore, the model assumes minimum fluidization conditions for the annulus. The solids circulation experiments showed that the annulus is probably below the minimum fluidization velocity. Therefore, the model calculates with an upward gas velocity in the annulus that is too high, which implies an underprediction of the temperature gradient. Model simulations showed, however, that the sensitivity of the temperature gradient in the annulus toward the gas velocity in the annulus is small. The input for the solids circulation rate is much more important.

In Figure 19, M_w, M_n, and M_w/M_n of the formed polymer are presented as functions of time for the experiment at 25.1 cm/s. This experiment shows the highest temperature gradients (both in time and over the annulus), leading to the highest polydispersity of the final product compared to the experiments at higher gas velocity. As can be seen from Figure 19, both M_w and M_n are decreasing in time, while M_w/M_n is increasing in time. The polydispersity at the beginning of the experiment is around 2.56, reflecting the two-site model. However, the increase in M_w/M_n is very small, indicating that the temperature gradients are too small to see any widening of the molecular-weight distribution. Obviously, hydrogen is more effective in controlling the molecular-weight distibution.

Injection of hydrogen

In Figure 20 the normalized temperature profiles obtained from the experiments with an injection of hydrogen and the prediction of the model are presented. The model overpredicts the temperature increase after the hydrogen injection to a certain extent. Moreover, the temperature before the hydrogen injection is also somewhat overpredicted. The deactivation observed during the experiments, both before and after the injection of hydrogen, is higher than predicted by the model.

The calculated polydispersity vs. the time of the formed polymer is shown for each experiment in Figure 21. The polydispersity starts to increase directly after the injection of hydrogen. The molecular weight distributions of the final polymers are presented in Figure 22. It can be seen that the distribution moves from the lower average molecular weights (hydrogen injection after 12.5 min) to higher average molecular weights (hydrogen injection after 30 min).

The polymer obtained from the experiments is a mixture of the startup powder and the low molecular-weight polymer produced during the experiment. The molecular weight of the startup powder is about 300 kg/mol, but with a rather high

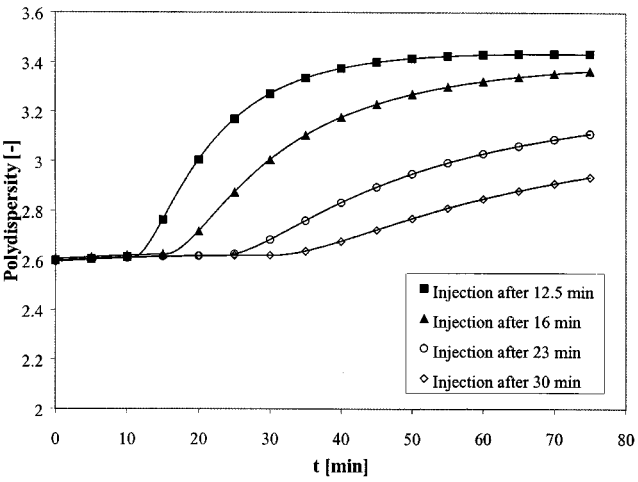

Figure 21. Model prediction of polydispersity as function of time for the experiments with injection of hydrogen.

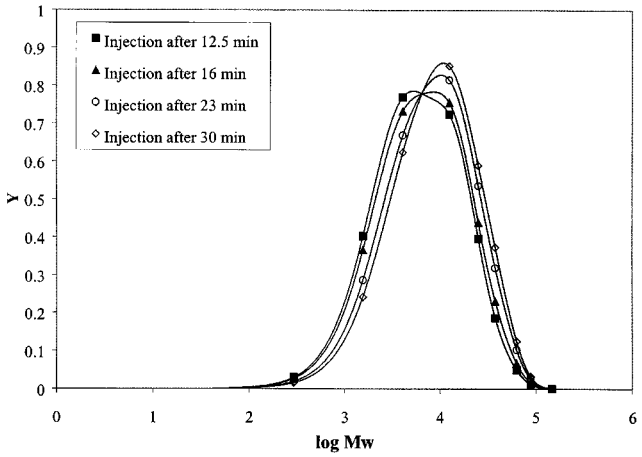

Figure 22. Model prediction of MWD of the final polymer for experiments with injection of hydrogen.

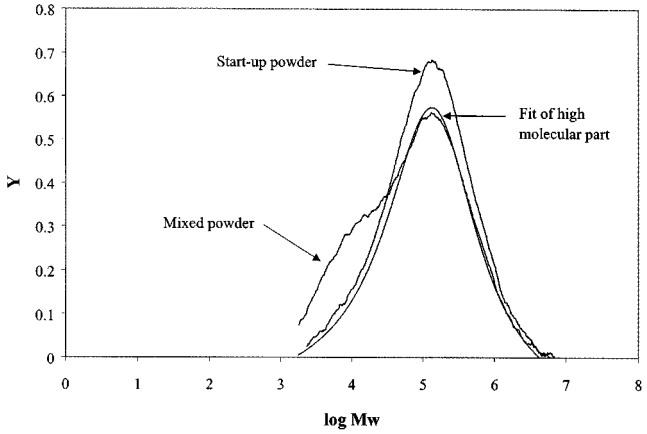

Figure 23. MWD of the startup powder, MWD of polymer obtained from an experiment with injection of hydrogen (startup powder and produced polymer), and MWD of startup powder used for subtraction.

polydispersity (about 7). The molecular-weight distribution of the startup powder is given in Figure 23. The GPC measurements of the mixed powders (startup material and its own produced polymer) were not very reproducible due to the low content of its own produced polymer in the samples obtained from the experiments (less than 10%). For one experiment (hydrogen injection after 24 min), a significant widening at the low molecular end of the original curve could be detected (see Figure 23). A fit of the molecular-weight distribution of the startup powder was subtracted from this curve in order to isolate the molecular-weight distribution from its own produced powder. Figure 24 presents the normalized subtracted distribution together with the prediction of the model for this experiment. Note that the errors of the subtracted distribution are quite large. Under these circumstances the experimental data are quite well represented by the model.

Discussion

The reactor system with the draft tube that was developed enables us to control the solids mixing required to study the polymerization of olefins in a small-scale fluidized-bed reactor. The temperature gradients caused by catalyst segregation observed when polymerizing without the use of the draft tube have not been found again. Moreover, elutriation of fines has not been observed despite the high gas velocities applied in the draft tube. The slugs rising through the draft tube (containing the entire particle-size distribution) probably carry the smaller particles to the annulus, thereby preventing serious elutriation.

When the draft tube is operated at high fluidization velocity, a better solid–gas heat transfer can be obtained compared to the classic bubbling fluidized-bed reactor, due to the higher slip velocity. A draft tube may also be interesting industrially, since the vertical solids mixing can be enhanced, thereby lowering the vertical temperature gradients. This is especially interesting when running in the condensed mode, where the maximum amount of liquid is (among others) limited by the vertical mixing (DSM, 2000). Recently, it was shown by Diepen and Mutsers (2001) that the draft tube concept can be applied under industrial conditions to improve the productivity of common gas-phase reactors for catalytic polymerizations. Up to 30% higher productivity has been observed. Another interesting effect is that higher H/D may be chosen, maintaining a stable fluidized bed, which provides engineering advantages, since these reactors are operated under pressure.

The three zones in the reactor with different heat transport properties may help to systematically broaden the molecular-weight distribution. However, the temperature gradients observed during a series of experiments in which the gas velocity was varied were too small to show a significant broadening.

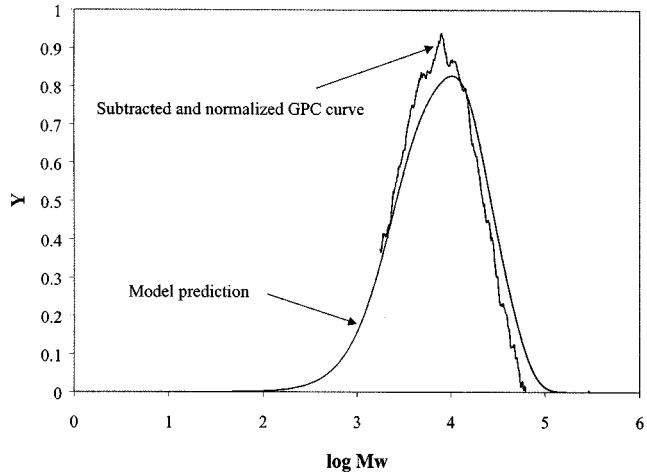

Figure 24. Model prediction of the MWD of a polymer from an experiment with injection of hydrogen and the distribution obtained after subtraction of the distribution of the startup powder.

The model presented uses the measured solids circulation characteristics as input data. If the model is to be used for scaleup, a model for the solids circulation rate should be included, which describes the circulation rate as a function of the gas velocity, reactor geometry, and so forth. Furthermore, the model should be improved by implementing the dynamics of monomer absorption and desorption in the polymer particles with related energy effects, thereby respecting the (changing) particle-size distribution.

Conclusions

Vertical particle mixing and segregation have been studied in a small-scale fluidized bed under pressure. At higher gas velocities, relatively fast mixing of tracer particles was found compared to the overall residence time of catalyst particles normally encountered in a polymerizing system. Particle-size analysis of samples taken at different vertical positions showed that the smaller particles accumulate in the upper zone of the bed.

Three semibatch polymerization experiments were executed at different fluidization velocities without using the draft tube. The phenomena observed during the mixing and segregation experiments were also observed during the polymerization experiments. It turned out that the catalyst particles accumulate in the upper zone of the bed, affecting the vertical temperature gradient. The speed of segregation is directly related to the mixing rate and therefore to the fluidization velocity.

The fluidized-bed reactor was equipped with a draft-tube and conical bottom section to control the solids mixing inside the reactor, thereby eliminating the problems observed before. The solids circulation rate was measured at different gas densities and gas velocities. It appeared that the particles in the draft tube and annulus part of the reactor move in plug flow. Slugging takes place in the draft tube and a moving-bed flow in the annulus. Segregation and elutriation of the fine particles, which were a dominant effect without the draft tube, could not be detected anymore during the operation with the draft tube.

Semibatch polymerizations were executed at different gas velocities, thereby varying the temperature gradients in the reactor from large to almost absent. Hydrogen was injected at different moments during the experiment in a special series of experiments. Directly after the hydrogen injection, temperatures increased due to the reactivation of dormant sites, causing a higher polymerization rate. Because the relative temperature increase after hydrogen injection is independent of the injection time, one can conclude that the relative concentration of dormant sites is constant during the experiment.

A compartment model was developed that is able to describe the generally unstable temperature profiles in the reactor and related molecular-weight distribution of the polymer. The underprediction of the temperature gradient over the annulus is probably due to the inaccuracies in the input data for the solids circulation rate. The solids circulation rates were measured under nonpolymerization conditions, while during polymerization, a sticky polymer was formed that limits the mobility of the powder.

The prediction of the model for the molecular-weight distribution could be checked for a single experiment. In this case, the prediction of the molecular-weight distribution was in reasonable agreement with the experimental result.

Acknowledgment

This work has been funded by BRITE-EURAM Project CATAPOL (BE 96-3022). The authors wish to thank DSM Research for the GPC measurements and materials they provided. We greatly acknowledge the technical team of the High Pressure Laboratories. M. J. Mollenhorst, A. A. van Klaveren, N. F. Geijsen, M. Poortenga, J. M. Rutten, and M. J. M. Hattink are acknowledged for their contribution in the experimental part.

Notation

A = cross-sectional area, m^2
C = amount of nonactivated catalyst, kg
C^* = amount of activated catalyst, kg
C_m = monomer concentration in polymer, kg/m^3
C_p = heat capacity, J/kg·K
d = thickness, m
$E_{act,d}$ = activation energy for deactivation, J/mol
$E_{act,i}$ = activation energy for initiation, J/mol
$E_{act,p}$ = activation energy for propagation, J/mol
ΔH_r = heat of reaction, J/kg
j = chain length
k_d = reaction-rate constant for deactivation, s^{-1}
k_i = reaction-rate constant for initiation, s^{-1}
k_p = reaction-rate constant for propagation, $m^3/kg \cdot s$
M_n = number averaged molecular weight, g/mol
M_w = weight-averaged molecular weight, g/mol
m^m = mass fraction of monomer
N = total number of compartments
N_n = nth moment of the MWD
p = pressure, bar
q = chain transfer probability
R = gas constant, J/mol·K
R_p = reaction rate, kg/s
t = time, s
T = temperature, K
T_∞ = temperature in air thermostat, K
u = velocity, m/s
U_{mf} = minimum fluidization velocity, m/s
U_e = inlet gas velocity, m/s
V = volume, m^3
X = mass fraction
y_j^d = density function of the instantaneous MWD

Greek letters

α = heat transfer coefficient, $W/m^2 \cdot K$
ϵ = void fraction
ρ = density, kg/m^3
ϕ_m = mass flow, kg/s

Subscripts or superscripts

a = annulus
av = average value
c = cone
comp = compartment
d = draft tube
e = conditions at reactor entry
g = gas
i = compartment number
m = monomer
p = polymer
r = reactor
s = solids
w = wall
0 = initial value

Abbreviations

MAO = methylaluminoxane
MWD = molecular-weight distribution
TIBA = tri-isobuthylaluminium

Literature Cited

Alappat, B., and V. C. Rane, "Effects of Draft Tube Height on Solids Circulation Rate and Particle Residence Time in a RCFB," *Ind. J. Eng. Mater. Sci.*, **2**, 113 (1995).

Berruti, F., J. R. Muir, and L. A. Behie, "Solids Circulation in a Spouted-Fluid Bed with Draft Tube," *Can. J. Chem. Eng.*, **66**, 919 (1988).

Choi, K. Y., and W. H. Ray, "The Dynamic Behavior of Fluidized Bed Reactors for Solid Catalyzed Olefin Polymerization," *Chem. Eng. Sci.*, **40**, 2261 (1985).

Daubert, T. E., and R. P. Danner, "Data Compilation of Pure Compounds," DIPPR Project, AIChE, New York (1985).

Diepen, P. J., and S. Mutsers, "Draft Tube Technology for Gas Phase Polypropylene Process Towards a Hypercondensed Mode Process," Dechema Monographs, Vol. 737, Wiley-VCH Verlag GmbH, Germany, p. 477 (2001).

DSM, WO Patent 00/69552 (2000).

Floyd, S., K. Y. Choi, T. W. Taylor, and W. H. Ray, "Polymerization of Olefins Through Heterogeneous Catalysis: III. Polymer Particle Modeling with an Analysis of Intraparticle Heat and Mass Transfer Effects," *J. Appl. Poly. Sci.*, **32**, 2935 (1986).

Ji, H., A. Tsutsumi, and K. Yoshida, "Solids Circulation in a Spouted Bed with a Draft Tube," *J. Chem. Eng. Jpn.*, **31**(5), 842 (1998).

Matsen, J. M., "Scale-up of Fluidized Bed Processes: Principles and Practice," *Powder Technol.*, **88**, 237 (1996).

McAuley, K. B., J. P. Talbot, and T. J. Harris, "A Comparison of Two Phase and Well-Mixed Models for Fluidized Bed Polyethylene Reactors," *Chem. Eng. Sci.*, **49**, 2035 (1994).

Meier, G. B., G. Weickert, and W. P. M. van Swaaij, "Gas-Phase Polymerization of Propylene: Reaction Kinetics and Molecular Weight Distribution," *J. Polym. Sci. A: Polym. Chem.*, **39**, 500 (2001a).

Meier, G. B., G. Weickert, and W. P. M. van Swaaij, "Comparison of Gas and Liquid Phase Polymerization with a Heterogeneous Metallocene Catalyst," *J. Appl. Poly. Sci.*, (2001b).

Montell Technology, U.S. Patent No. 5,698,642 (1997).

Samson, J. J. C., G. Weickert, A. E. Heerze, and K. R. Westerterp, "Liquid Phase Polymerization of Propylene with a Highly Active Catalyst," *AIChE J.*, **44**, 1424 (1998).

Song, B. H., Y. T. Kim, and S. D. Kim, "Circulation of Solids and Gas Bypassing in an Internally Circulating Fluidized Bed with Draft Tube," *Chem. Eng. J.*, **68**, 115 (1997).

Talbot, J. P., "The Dynamic Modeling and Particle Effects on a Fluidized Bed Polyethylene Reactor," PhD Thesis, Queen's Univ., (1990).

Yang, W. C., and D. Keairns, "Studies on the Solid Circulation Rate and Gas Bypassing in Spouted Fluid-Bed with a Draft Tube," *Can. J. Chem. Eng.*, **61**, 349 (1983).

Manuscript received Apr. 26, 2001, and revision received Nov. 12, 2001.